# 動的荷重에 의한 重力式 옹벽의 永久變位

## Permanent Gravity Retaining Wall Displacement Due to Dynamic Loads

金 成 敎*
Kim, Sung Kyo

### 摘 要

Mononobe-Okabe에 의해서 옹벽에 대한 動的 土壓計算法이 開發된 이래 本論題中 옹벽의 滑動에 의한 變位에 대해서는 많은 硏究가 이루어졌으나 Mononobe-Okabe式이 元來 옹벽 自體의 慣性을 고려치 아니하였고 또 動的 荷重의 작용점을 제시하지 않으므로서 전도모멘트를 계산할 수 없게 하므로서 옹벽의 전도에 의한 變位에 대해서는 硏究가 되지 아니하였다.

本 硏究의 目的은 해석적 방법과 모형실험을 통해서 지진 및 폭파 등의 動的 荷重에 의한 옹벽의 전도에 의한 變位를 고찰하고자 하는 바 그 結果를 要約하면 다음과 같다.

1. 활동에 대한 항복가속도가 있는 것과 마찬가지로 전도에 대한 항복가속도가 있다. 이 항복가속도는 옹벽의 안전율이 증가함에 따라 증가한다.
2. 理論値와 實驗値는 경향으로 보아 일치한다. 실험치가 이론치보다 작은 것은 모형실험에서 옹벽측면과 컨테이너 사이의 마찰에 기인한 것으로 보아지며 마찰을 줄임으로써 이론치에 더 접근시킬 수 있을 것이다.
3. 옹벽의 회전각도의 크기는 지반가속도가 클수록, 옹벽저면이 작을수록 그리고 흙의 내부마찰각이 작을수록 크게 증가한다.
4. 실용적인 규격의 옹벽의 변위는 활동에 의한 것보다 전도에 의한 것이 훨씬 크며 전체 변위의 대부분을 차지한다.
5. 옹벽 상단의 횡적 변위는 옹벽 설계를 결정짓는 중요한 요소가 될 수 있다.

## 1. Introduction

Dynamic lateral forces on earth retaining structures usually result from three main causes; earthquakes, explosions and vehicular traffic. The dynamic effects of moving loads, such as vehicles, are often small and can readily be taken into account in design by the application of appropriate equivalent surcharge or line loads. Thus it is the loads resulting from earthquakes and explosions which pose the greatest problems for the design of earth retaining structures.

Retaining walls designed for earthquakes effects may be grouped into two main categories on the basis of their failure mode:

1. Gravity retaining walls, using the mass of the wall for stability, which fail by sliding or by overturning. These may be called displacement-governed walls. The internal force levels in such walls are of secondary importance.
2. Cantilever, tied-back or braced walls, which fail by fracture or yield of one of the structural components involved. These may be called force-governed walls. For at least

* SOILS INTERNATIONAL, Consulting Foundation Engineers and Geologists

some part of such structural systems the internal force level is important.

This paper deals with the displacement of gravity retaining walls, the first category, due to earthquakes.

Very informative overviews on the subject can be found in the works by Seed and Whitman (1970), Nazarian and Hadjian(1979), and Prakash(1981). In the previous studies of the subject, the rotational movement of the walls and the inertia force of the walls have been ignored or addressed inadequately in evaluating the lateral displacements of a wall caused by ground accelerations. It does not mean that the rotation is insignificant. The fundamental reason for not addressing the wall rotation is that the Mononobe-Okabe method does not give the location of the dynamic force, making it difficult to correctly evaluate the overturning moment.

The objective of this study is to establish that the rotational movement of retaining walls during earthquakes can not be ignored as evaluated in past studies by previous investigators or even it contribute the major part of the displacement of the top of the walls.

To evaluate permanent rotations of gravity retaining walls, small scale laboratory tests were conducted using, as model walls, rectangular gravity retaining walls whose factors of safety aginst rotation vary from 1.43 to 2.23. Mononobe-Okabe's dynamic earth pressure and wall inertia force were considered in establishing the equation of motion.

## 2. Past study

Many experimental studies, since the dynamic lateral pressure on a retaining structures was developed by Mononobe(1929) and Okabe(1926), have been conducted on small walls to understand the physical behavior of retaining walls and to obtain tentative data on the increases in earth pressures and their points of application. The basic principle of earth pressure experiments has been to simulate the strain conditions in backfill and thus treat the setup as a small prototype. Some of the major past studies among many are summarized in the following.

### Mononobe-Okabe Seismic Coefficient Analysis

Being probably the earliest method for determining the dynamic lateral pressure on a retaining structure, the Mononobe-Okabe analysis is a straightforward extension of the Coulomb sliding wedge theory where quasi-static vertical and horizontal inertia forces of the sliding wedge are included. A complete review of the procedure has been given by Seed and Whitman (1970). Only active case will be summarized here.

Consider the combined free-body diagram shown in Fig.1 where the failure surface OA creates a sliding wedge of weight $W_s$ with inertial components $K_hW_s$ and $K_vW_s$. Force equilibrium of the wedge alone(Fig. 2), gives the basic Mononobe-Okabe formula for total

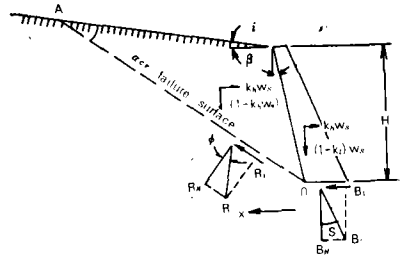


**Fig. 1. Combined Force Diagram: Active Case**

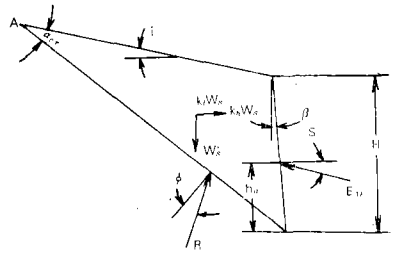


**Fig. 2. Active Wedge**

active thrust:

$$P_{AE}=1/2\,\gamma H^2(1-K_v)\,K_{AE}$$

Where

$$K_{AE}=\frac{\cos^2(\phi-\theta-\beta)}{\cos\theta\cos^2\beta\cos(\delta+\beta+\theta)\left[1+\sqrt{\frac{\sin(\phi+\delta)\sin(\phi-\theta-i)}{\cos(\delta+\beta+\theta)\cos(i-\beta)}}\right]^2}$$

$\theta=\tan^{-1}k_h/(1-k_v)$

$\gamma$=unit weight of soil

$H$=height of wall

$\phi$=angle of friction of soil

$\delta$=angle of wall friction

$i$=slope of ground surface behind wall

$\beta$=slope of bach of wall to vertical

$K_h$=horizontal ground acceleration/g

$K_v$=vertical ground acceleration/g

The horizontal component of the force $P_{AE}$ may be expressed as $P_{AEh}$ where $P_{AEh}=P_{AE}\cos(\delta+\beta)=1/2\,\gamma H^2(1-K_v)\cdot K_{AE}\cos(\delta+\beta)$. No satisfactory analytical solution appears to exist for the location of the dynamic lateral force. They apparently considered that the resultant of the dynamic pressure computed by their analytical approach would act on the wall at the same position as the initial static pressure; that is, at one third of the wall height above the base. The inertia force of the wall has also been ignored in force equilibrium.

In the test setup of Mononobe and Matsuo (1929), a box was mounted on a horizontal shake table, filled with dry sand, and subjected to different acceleration levels by exciting the table. The maximum pressures exerted on the wall of the box were measured by means of hydraulic gauges. It was concluded that the maximum pressure increased with base acceleration and the values essentially agreed with those computed by the Mononobe-Okabe formula.

In the test setup of Matsuo and O'Hara (1960), 40-cm-high walls were excited with vibration for a period of 0.3s. On fixed walls, it was found that the amplitude of pressure change is large at midheight. In 5-m-high concrete walls which were excited by a 1-hp oscillator mounted in a trough sunk in the ground 4.5m. away from the wall, pressures were measured on pressure cells. Larger pressures were observed with increasing ground accelerations, with peak pressures at about one-third of the way from the top of the wall.

Murphy (1960) conducted tests on a solid rubber model of a gravity wall to study the qualitative behavior of backfill during vibrations, and found that the slip surface that developed was flatter than the slip surface under static conditions. The slip surface at Shinizu Harbor, developed in 1930, probably had almost the same inclination.

## Richards AND ELM'S ANALYSIS

Recognizing movements of the walls as another important aspect of the gravity retaining wall design, Richards and Elms (1979) applied Newmark's method (1965) to evaluate the accumulated lateral displacement of a wall caused by ground accelerations. Retaining walls then can be designed according to an acceptable magnitude of the wall displacement. In their method, a rigid plastic backfill was assumed and only the permanent displacement is considered. If, during shaking, the ground acceleration was inward toward the backfill, the wall inertia is thus outward. At the time, an acceleration level exceeds a certain limit, the wall will yield and move relatively with respect to the ground under an active case. However, the displacement does not continue indefinitely, but stops as soon as the ground acceleration reverses its direction to make a zero relative velocity between the wall and the ground. Only the outward displacement under the active case is considered because the passive failure is considered unlikely. The accumulated outward movement is the total wall displacement of the wall. No rotational movement was considered in this method.

Sim and Berrill (1979) conducted shaking table tests of a model gravity retaining wall to verify the general correctness of the Ric-

hards and Elms' theoretical model, and to check the validity of Richards and Elms' method of predicting the lateral permanent displacements of the walls. Furthermore, with one exception, it appears that the detailed assumptions of the model are correct. The assumed constant post-yield acceleration was not seen in the laboratory tests, but the linear relationship observed between ground and wall accelerations should be easily incorporated into the model. However, the model wall used in their experiments was deliberately made to eliminate rotation by making the wall base very wide and the center of gravity very low, which can not be expected to represent actual retaining walls.

Considering reinforced earth walls to be designed by limit state procedures, Rea and Wolfe (1980) devised an idea that during strong earthquakes excitation, the factors of safety of such walls, like other earthern structures, may become momentarily less than unity. Since the factors of safety are less than unity for only short periods of time, the walls do not necessarily fail; however, they accumulate permanent deformations. Therefore, it would be desirable to add to the limit design procedure a requirement restricting the permanent displacements that reinforced earth walls could incur during earthquakes.

The 12 in, 18 in, and 24 in, high walls were constructed with plexiglass face elements, 1/2 inch wide mylar tape reinforcing ties, and a clean fine sand. The earthquake motion used in the experiments was derived from the N 21 E component of the Taft (1952) earthquake.

The results for experiments involving 18 inch walls showed that a reinforced earth wall subjected to earthquake motions at low levels of intensity responds like a continuous elastic body. At high intensity levels, however, it responds like a rigid body resting on a horizontal surface vibrating horizontally, with the exception that slippage occurs for a much smaller acceleration in one direction than for acceleration in the other direction. The acceleration at which slippage occurs, the yield acceleration, and the magnitude of earthquake-induced permanent displacements depend principally on the static factor of safety of the walls.

## 3. Analysis

Referring to Fig. 3, the ground acceleration

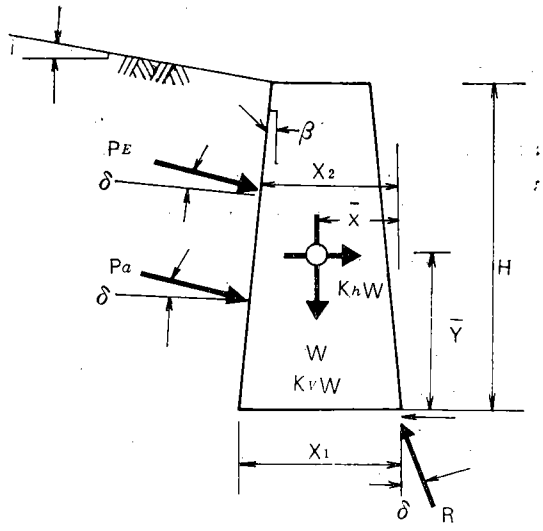


(a) M-O Model

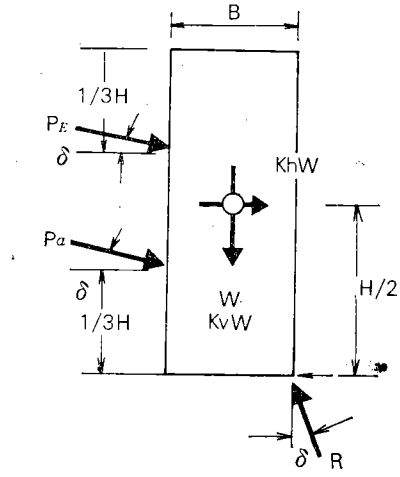


(b) Model wall

**Fig. 3. Mononobe-Okabe Force Diagram**

imparts a dynamic earth pressure as well as inertia force on the wall. If, during shaking, the ground acceleration is inward toward the backfill, the wall inertia is thus outward. At the time an acceleration level exceeds a certain limit, the wall will yield and move relatively with respect to the ground under an active case. However, the displacement does not continue indefinitely, but stops as soon as the ground acceleration reverses its direction to make a zero relative velocity between the wall and the ground. Only the outward displacement under the active case is considered because the passive failure is considered unlikely. The accumulated outward movement is the total wall displacement of the wall.

Equations of motion for lateral translation and rotation can be established for a wall as follows, assuming that the center of rotation is at the toe of the wall where the reaction on the wall base acts at the time of rotation.

For sliding:

$$P_{AEh}+K_hW-(W+K_vW+P_{AEv})\tan\delta=\frac{W}{g}\bar{a} \quad \cdots\cdots(1)$$

For rotation;

$$P_{ah}\frac{1}{3}H+P_{Eh}\frac{2}{3}H+K_hW\bar{y}-P_{av}x_1-P_{Ev}x_2 -(1+K_v)W\bar{x}=I\alpha+\frac{W}{g}\bar{a}\bar{y} \quad \cdots\cdots(2)$$

and the dynamic increment $P_E$;

$$P_E=P_{AE}-P_a \quad \cdots\cdots(3)$$

in which $P_a$ is the static active force, and $P_{AE}$ is the total dynamic force according to M-O;

$$P_{AE}=\frac{1}{2}\gamma H^2(1-K_v)K_{AE} \quad \cdots\cdots(4)$$

Where

$$K_{AE}=\frac{\cos^2(\phi-\theta-\beta)}{\cos\theta\cos^2\beta\cos(\delta+\beta+\theta)\left[1+\sqrt{\frac{\sin(\phi+\delta)\sin(\phi-\theta-i)}{\cos(\delta+\beta+\theta)\cos(i-\beta)}}\right]^2}$$

$K_{AE}$=dynamic active pressure coefficient plotted in Fig. 4.

$\theta=\tan^{-1}\frac{K_h}{1-K_v}$

$W$=wall weight

$K_h, K_v$=horizontal and vertical seismic coefficients

$B$=wall width

$H$=wall height

$\bar{I}$=moment of inertia of walls

$\bar{a}, \alpha$=linear and angular accelerations of walls

$x's, y's$=coordinates shown in Fig. 3

$\beta$=slope of the wall to the vertical

$i$=backfill slope

$\gamma$=unit weight of soil

$\phi$=angle of friction of soil

$\delta$=friction angle between the base and soil=$\frac{2}{3}\phi$

In many earthquakes, the vertical ground acceleration is small and often negligible. It is therefore omitted in this study.

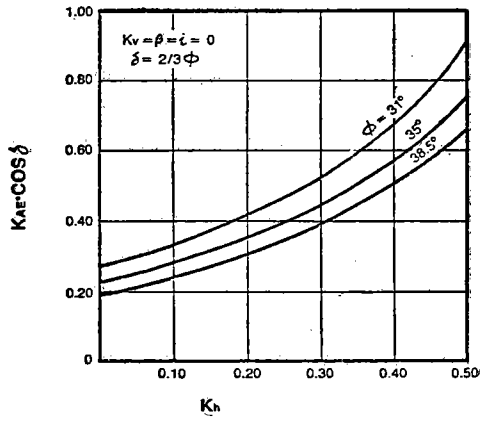


**Fig. 4. Dynamic Active Pressure Coefficient**

The linear and angular acceleration $\bar{a}$ and $\alpha$ can be solved from equation 1 and 2; however, walls do not necessarily start to slide or rotate as soon as the ground accelerations start. The factors of safety required in design prevent relative motion or rotation of the wall until certain levels of the ground accelerations, called the yield accelerations, are reached. The sliding and the rotational yield accelerations which are the levels of the ground accelerations at which either sliding or rotation is about to begin can be obtained by solving for $K_h$ in equations 1 and 2 when the right hand side of the equations

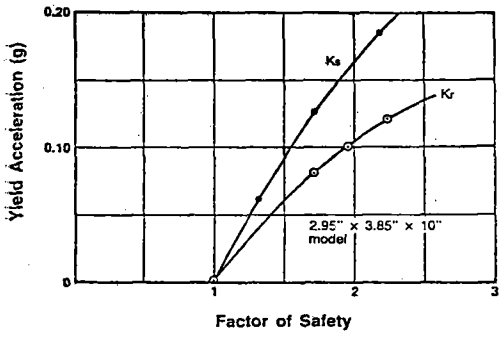


**Fig. 5. Yield Acceleration.**

are zeros. These values for the model walls used are listed in Table-5. Fig. 5 shows the yield acceleration vs. static factor of safety against sliding and overturning for the largest model wall. Rea and Wolfe (1980) experimentally found the sliding yield accelerations of reinforced earth walls and obtained the general trend shown by Fig. 5, but their factor of safety was defined for the metal strips used in the tests.

Equation 2 for the model walls is reduced to:

$$P_{ah}\frac{1}{3}H+P_{EH}\frac{2}{3}H+K_h W\frac{H}{2}-(P_{av}+P_{EV})B -W\frac{B}{2}=\bar{I}\alpha+\frac{W}{g}\bar{a}\frac{H}{2} \cdots\cdots\cdots(5)$$

in which $I=\frac{W}{12g}(B^2+H^2)$. The angular acceleration is then solved from equation 5 provided an equivalent $K_h$ value for each acceleration peaks which exceed the yield acceleration for rotation $K_r$ is known. To simplify the problem the commonly assumed sinusoidal ground acceleration is replaced by a constant step acceleration pulse having the same area as shown in Fig. 6. During the short interval when the equivalent acceleration is larger than the rotational yield acceleration the overturning moment will cause the wall to rotate with $\alpha$. If the equivalent ground acceleration $K_h$ is less than the sliding yield acceleration, no slip occurs and the linear acceleration $\bar{a}$ is replaced by $\frac{H}{2}\alpha$ for pure rotation. However, if $K_h$ is larger than $K_s$, the sliding yield acceleration, both rotation and sliding will occur simultaneously. The linear acceleration $\bar{a}$ is assumed at this time to be $K_s$ itself (Richards and Elms 1979). Angular velocity is obtained by a direct integration of the angular acceleration. The rotation stops when the angular velocity becomes zero because of the reversal of the direction of the acceleration. Fig. 6 shows a mirror image of angular velocity reduction for simplicity as suggested by Goodman and Seed (1966). The angular rotation is obtained by integrating the angular velocity in this interval. After a period of pause, the rotational process repeats for the next acceleration which is greater than the yield acceleration. The wall rotates by lurching until the last acceleration which exceeds the rotational yield acceleration resulting in a permanent rotation.

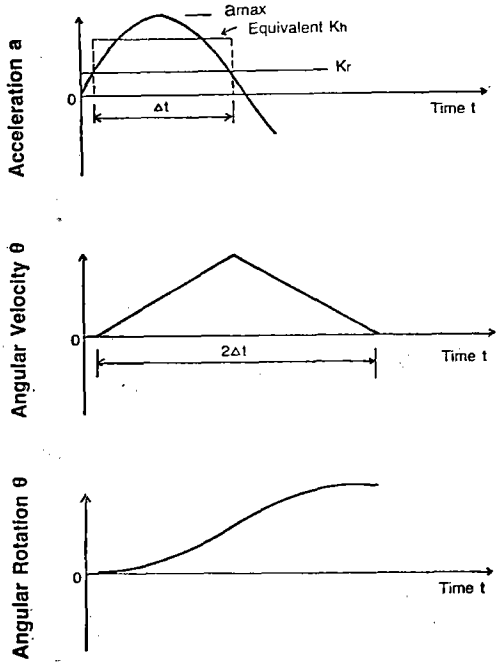


**Fig. 6. Angular Rotation**

## 4. Model Tests

Density trials were conducted first to produce uniform densities with varying drop height

**Table-1. Density Trials**

| Trial \ Drop Ht. | 15 inch | 9 inch | 6 inch | 2 inch |
|---|---|---|---|---|
| 1 st | 110.0 pcf. | 109.2 pcf. | 107.9 pcf. | 103.1 pcf. |
| 2 nd | 110.1 〃 | 108.5 〃 | 107.7 〃 | 102.6 〃 |
| 3 rd | 110.2 〃 | 108.8 〃 | 107.6 〃 | 103.8 〃 |
| Average | 110.1 〃 | 108.8 〃 | 107.7 〃 | 103.2 〃 |

**Table-2. Test Equipments**

| | ITEM | MODEL | USAGE |
|---|---|---|---|
| 1. | M.B. Control Panel | M.B. C-10/3200 | Control Systems |
| 2. | Oscilloscope | T 912 | Frequency Measurement |
| 3. | Amplifier | M.B. N 400 | Acceleration Indicator |
| 4. | Shaker | C 10 E | Shaking the Shaking table |
| 5. | Shaking table | 2020-Al-3 | Shaking container |
| 6. | Accelerometer | | Picking up Acceleration |

from 2 inch to 15 inch as shown in Fig. 7. The standard 20-30 Ottawa sand was used. The sand was dropped freely through a #8 screen attached to the top of $1\frac{1}{2}$ inch (38mm) plastic pipe. They are tabulated in Table-1. Drop heights 15 inch, and 9 inch were chosen for the tests to produce 110.1 and 108.8 lb. per cu. ft. (17.29 and 17.10 KN/m$^3$) respectively. The loosest density of 103.2 lb per cu. ft (16.19 KN/m$^3$) was obtained by directly pouring the sand gently with a scoop instead of using 2 inch-high pipe. The angles of internal friction obtained by the direct shear test 34, 32.5 and 31 degrees corresponding to the above densities. They were lower than the values surveyed by Lee and Singh (1968). The average values according to Lee's survey were 38.5, 35, and 31 degrees for these densities. These latter values were used in all the analysis.

The equipments used in the tests are shown in Table-2.

The model walls which are 10 in. (254mm) high, 3.85 inch (98mm) long with various widths were made of portland cement mortar as shown in Fig. 8. A 16×24×4 inch (406×610×102mm) container of 3/4 inch (19mm) thick plexiglass was firmly attached to the shaking table of a M.B. Electronic shaker (M.B.C-10/3200). Each density was set up according to the test schedule (Table-3), using the same standard 20-30 Ottawa sand for each test in which a different acceleration was applied. To avoid the sand particles flowing into the gaps between the model wall and the container walls, thin strips of styrofoam were pasted on both sides of the model walls. An accelerometer was attached to the head of the shaker while another one was either burried in the sand 6 inches (152mm) from the model walls and one inch (25.4mm) below the ground surface or attached on the container wall $10\frac{1}{4}$ inches (260mm) above the base. A typical set-up is shown in Fig. 9.

The lowest frequency for sinusoidal accelerations that the shaker can be operated without severe distortion of the acclerograms recorded at the shaker's head was about 15 cps for the experimental set-up. This frequency was used in the tests but the actual frequency for each

**Table-3. Test Schedule**

| Density \ Model wall | 2.3 inch | 2.5″ | 2.7″ | 2.95″ |
|---|---|---|---|---|
| 110.1 pcf. | X | | | X |
| 108.8 〃 | | X | | X |
| 103.2 〃 | | | X | |

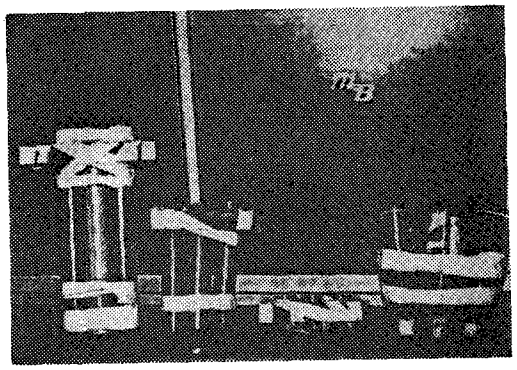

Fig. 7. Piper and Funnel for density set-up

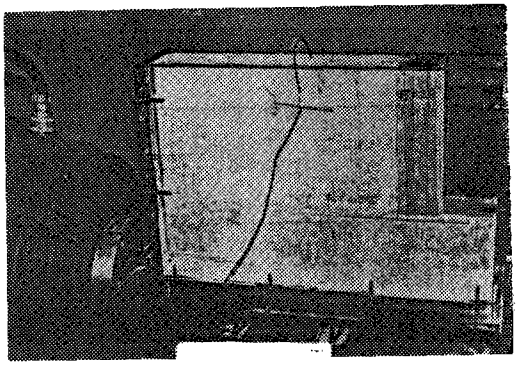

(a) Before test

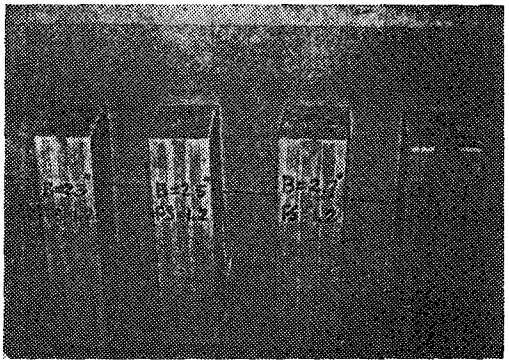

Fig. 8. Model Walls

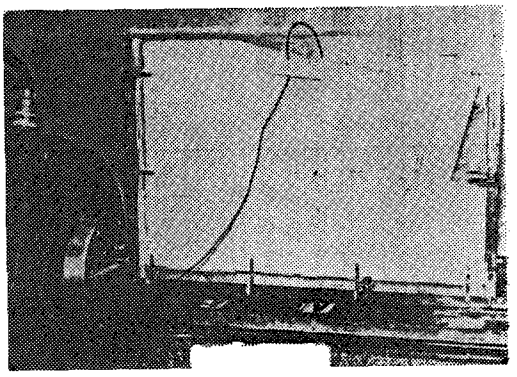

(b) After test

Fig. 9. Model test set-up

test was calculated from the recorded accelerograms (T912). Different levels of constant sinusoidal accelerations were applied and the wall rotation, lateral displacement and the time intervals were recorded. Test results are listed in Table-4.

## 5. Results and Discussion

Table-4 shows all the tentative data. As shown in last three columns of Table-4, one or more than one angle of rotation for each test were recorded by time interval. If the rotation was large enough, the initial configuration on which the equations of motions were established might no longer hold. Therefore, if there are more than one angle of rotations recorded for one test, angle of rotation was chosen for the calculation of rotation per cycle, such that it is less than 10 degrees or lines up with the adjacent points of different accelerations. The rotational angle per one cycle can then be calculated. Columns (13), (14), (15), in Table -5 were rearranged from Table-4 in such a way and these values (column 15 in Table-5) were plotted against the applied accelerations as shown in Fig. 11.

Referring to accelerations in Tables 4, 5, accelerations were taken at the container wall and the head of the shaker in the beginning stages of these tests. In order to have correlation between acceleration at the container wall and the ground acceleration in the sand, a series of measurements were performed. These correlations are shown in Fig. 10. The accelerations taken at the container wall in some of the tests were all converted to the equivalent ground acceleration in the sand according to Fig. (10) as shown in Tables 4, 5. This ground

**Table-4. Test Results**

| Base Width (in) | Density (pcf) | Friction Angle (°) | Acceleration (g's) | | | Frequency | Data | | |
|---|---|---|---|---|---|---|---|---|---|
| | | | $a_{sand}$ | $a_{box}$ | $a_{head}$ | (cps) | Time (sec) | Angle of Rotation (°) | Displacement (cm) |
| 2.3 | 110.1 | 38.5 | 0.062* | 0.07 | 0.07 | 16.7 | No Displacement | | |
| | | | 0.072* | 0.08 | 0.08 | 16.7 | 16 | 5 | 2.2 |
| | | | | | | | 20 | 10 | 4.5 |
| | | | | | | | 22 | 16 | 7.0 |
| | | | 0.090* | 0.10 | 0.11 | 16.7 | 5 | 4 | 1.5 |
| | | | 0.125* | 0.14 | 0.15 | 16.7 | 4 | 5 | 2.2 |
| | | | | | | | 6 | 10 | 4.5 |
| | | | | | | | 7 | 16 | 7.0 |
| | | | 0.153* | 0.17 | 0.18 | 16.7 | 4 | 16 | 7.0 |
| 2.5 | 108.8 | 35 | 0.072* | 0.08 | 0.10 | 16.7 | No Displacement | | |
| | | | 0.134* | 0.15 | 0.15 | 16.7 | 5 | 2.5 | 1.4 |
| | | | | | | | 10 | 8 | 3.2 |
| | | | | | | | 15 | 16 | 7.0 |
| | | | 0.160* | 0.18 | 0.21 | 17.2 | 5 | 11.5 | 5.3 |
| | | | | | | | 8 | 16 | 7.0 |
| | | | 0.242* | 0.27 | 0.32 | 16.7 | 2.6 | 16 | 7.0 |
| 2.7 | 103.2 | 31 | 0.067* | 0.075 | 0.09 | 17.2 | No Displacement | | |
| | | | 0.085* | 0.095 | 0.11 | 17.2 | 5 | 3.5 | 1.6 |
| | | | | | | | 10 | 6.5 | 3.0 |
| | | | | | | | 15 | 12.5 | 5.7 |
| | | | | | | | 17.8 | 16 | 7.0 |
| | | | 0.107* | 0.12 | 0.14 | 17.2 | 5 | 7 | 3.1 |
| | | | | | | | 10 | 16 | 7.0 |
| | | | 0.140 | 0.16 | 0.20 | 16.7 | 6.2 | 13 | 6.6(0.8) |
| | | | 0.170 | 0.19 | 0.23 | 16.7 | 3.9 | 12 | 6.6(1.2) |
| 2.95 | 110.1 | 38.5 | 0.134* | 0.15 | 0.19* | 16.0 | No Displacement | | |
| | | | 0.178* | 0.20 | 0.24 | 17.2 | 5 | 3 | 1.2 |
| | | | | | | | 20 | 9 | 3.8 |
| | | | | | | | 25 | 17 | 7.0 |
| | | | | | | | 30 | 25 | 11.0 |
| | | | 0.223* | 0.25 | 0.29 | 17.2 | 2.2 | 5 | — |
| | | | | | | | 5 | 16 | — |
| | | | 0.242* | 0.27 | 0.40 | 15.6 | 7.2 | 10 | 6.6(2.0) |
| | | | 0.250* | 0.28 | 0.38 | 16.1 | 5.5 | 12.5 | 6.6(1.1) |

| | | | | | | | | | |
|---|---|---|---|---|---|---|---|---|---|
| 2.95 | 108.8 | 35 | 0.134* | 0.15 | 0.19 | 16.7 | No Displacement | | |
| | | | 0.178* | 0.20 | 0.26 | 16.7 | 10<br>20 | 6<br>8 | 2.4<br>3.1(1.0) |
| | | | 0.223* | 0.25 | 0.31 | 17.2 | 10<br>20 | 10<br>15 | 4.2<br>6.5 |
| | | | 0.242* | 0.27 | 0.35 | 16.7 | 5 | 15 | 0.5 |

* ; Converted from Fig. 10.
( ) ; Denotes displacement of base of walls.

acceleration was used for the "Experimental" curves in Fig. (11).

At lower levels of acceleration, the walls moved by rotation only, but at higher levels the walls rotated and slid. However, the sliding motion was not apparent. The rotational movements were severe enough that the toes of the walls dug into the sand while the heel tilted up creating a small pocket of empty space between the base of the wall and the sand. Sand particles were observed to flow into the pocket as the walls rotated. The heel of the walls made traces of arc moving upward and outward under severe shaking. If the rotation was large enough the initial configuration on which the equations of motions were established might no longer hold. The digging action of the toes into sand could have retarded the lateral movement of the walls. In many cases, the top of the walls moved excessively due to rotation of walls without the pure lateral displacement of the wall base. In the theoretical calculations, no sliding was assumed based on this observation. Therefore, despite the equivalent ground acceleration $K_h$ is larger than $K_y$, the sliding yield acceleration, the linear acceleration $\bar{a}$ is not assumed to be equal to $K_y$ as in Richard's and Elms' method, but it is replaced by $\frac{H}{2}\alpha$ as in the case for pure rotation. Namely, yield accelerations for sliding in column (7) of Table-5 were not used in the theoretical calculations.

The total angle of rotation for a given accelerogram can be calculated by summing up the angle of rotation created by each acceleration peak which exceeds the yield acceleration for rotation. This principle is applicable to all types of acceleration including those by earthquakes. The lateral displacement of the top of a wall is the product of sine of the total angle of rotation and the wall height. The analytical method based on the equation of motion as proposed in this paper may be used to predict the wall movements, but it may give a conservative answer as indicated by the experimental results shown in Fig. 11. These curves are rearranged for convenient use in Fig. 12.

**EXAMPLE:**

A rectangular gravity retaining wall 20 ft. high, 5 ft. wide supports a horizontal backfill which has $\phi=35$ degree, $\delta=23.3$ degree, $\gamma=108.8$ lb/ft$^3$ (16.82KN/m$^3$). If the wall is subjected to a severe earthquake which has 10 cycles of equivalent sinusoidal acceleration with $A_{max}=0.12g$ and 4 cps, how large displacement would

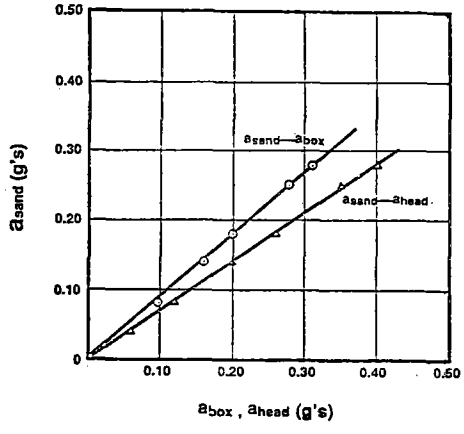


**Fig. 10. Correlations Between Accelerations**

**Table-5. Test Results**

| Base width $B$ (in) (1) | Density $\gamma$ (pcf) (2) | Friction angle $\phi$ (°) (3) | Active coeffi-cient $K_a$ (4) | yield acceler-ation rotation $K_r$ (5) | Factor of safety rotation $FS_r$ (6) | Yield acceler-ation sliding $K_s$ (7) | Factor of safety sliding $FS_s$ (8) | Acceleration(g's) $a_{sand}$ (9) | $a_{box}$ (10) | $a_{head}$ (11) | Frequency (cps) (12) | Time (sec) (13) | Angle of rotation $\theta$ (°) (14) | Rotation per cycle 0/cycle °/cycle (15) |
|---|---|---|---|---|---|---|---|---|---|---|---|---|---|---|
| | | | | | | | | 0.062* | 0.07 | 0.07 | 16.7 | — | No Displacement | 0 |
| | | | | | | | | 0.072* | 0.08 | 0.08 | 16.7 | 16 | 5 | 0.019 |
| 2.3 | 110.1 | 38.5 | 0.213 | 0.05 | 1.43 | 0.14 | 1.76 | 0.090* | 0.10 | 0.11 | 16.7 | 5 | 4 | 0.048 |
| | | | | | | | | 0.125* | 0.14 | 0.15 | 16.7 | 6 | 10 | 0.100 |
| | | | | | | | | 0.153* | 0.17 | 0.18 | 16.7 | 4 | 16 | 0.240 |
| | | | | | | | | 0.072* | 0.08 | 0.10* | 16.7 | — | No Displacement | 0 |
| 2.5 | 108.8 | 35 | 0.244 | 0.055 | 1.45 | 0.095 | 1.48 | 0.134* | 0.15 | 0.15 | 16.7 | 10 | 8 | 0.048 |
| | | | | | | | | 0.160* | 0.18 | 0.21 | 17.2 | 8 | 16 | 0.116 |
| | | | | | | | | 0.242* | 0.27 | 0.32 | 16.7 | 2.6 | 16 | 0.369 |
| | | | | | | | | 0.067* | 0.075 | 0.09 | 17.2 | — | No Displacement | 0 |
| | | | | | | | | 0.085* | 0.095 | 0.11 | 17.2 | 10 | 6.5 | 0.038 |
| 2.7 | 103.2 | 31 | 0.286 | 0.06 | 1.50 | 0.053 | 1.25 | 0.107* | 0.12 | 0.14 | 17.2 | 5 | 7 | 0.081 |
| | | | | | | | | 0.140 | 0.16 | 0.20 | 16.7 | 6.2 | 13 | 0.126 |
| | | | | | | | | 0.170 | 0.19 | 0.23 | 16.7 | 3.9 | 12 | 0.184 |
| | | | | | | | | 0.134* | 0.15 | 0.19* | 16.0 | — | No Displacement | 0 |
| | | | | | | | | 0.178* | 0.20 | 0.24 | 17.2 | 20 | 9 | 0.026 |
| 2.95 | 110.1 | 38.5 | 0.213 | 0.12 | 2.23 | 0.185 | 2.19 | 0.223* | 0.25 | 0.29 | 17.2 | 2.2 | 5 | 0.132 |
| | | | | | | | | 0.242* | 0.27 | 0.40 | 15.6 | 7.2 | 10 | 0.089 |
| | | | | | | | | 0.250* | 0.28 | 0.38 | 16.1 | 5.5 | 12.5 | 0.141 |
| | | | | | | | | 0.134* | 0.15 | 0.19* | 16.7 | — | No Displacement | 0 |
| 2.95 | 108.8 | 35 | 0.244 | 0.10 | 1.94 | 0.125 | 1.70 | 0.178* | 0.20 | 0.26 | 16.7 | 20 | 8 | 0.024 |
| | | | | | | | | 0.223* | 0.25 | 0.31 | 17.2 | 10 | 10 | 0.058 |
| | | | | | | | | 0.242* | 0.27 | 0.35 | 16.7 | 5 | 15 | 0.180 |

*; Converted from Fig. 10.

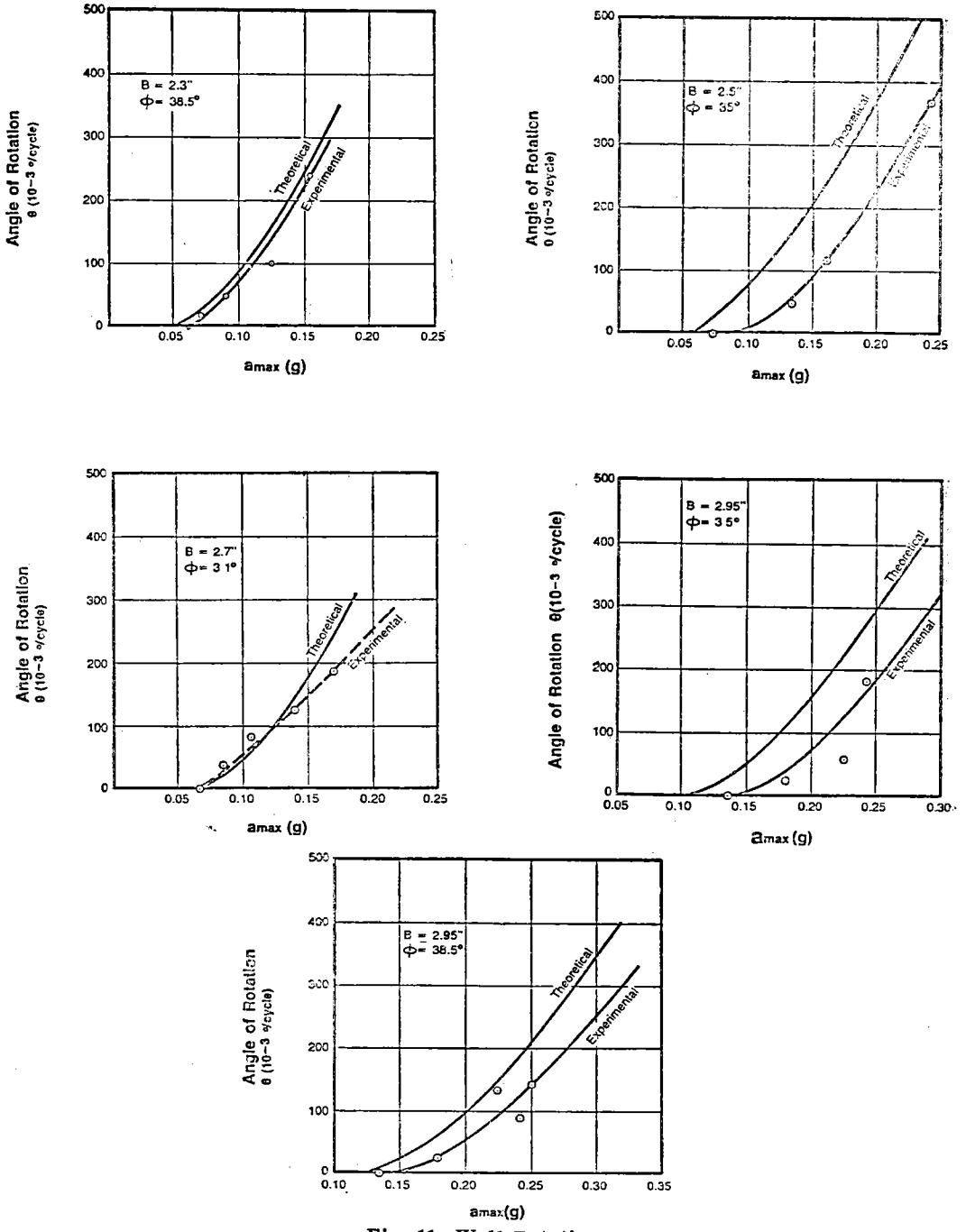


**Fig. 11. Wall Rotation**

the retaining wall experience at the top of the wall?

Solution;

The rotational yield acceleration for the wall which has Fs=1.45 against rotation is 0.055g. The equivalent step ground acceleration $K_h$= 0.1g. Substituting $P_{ah}$=4876, $P_{av}$=2100, $W$= 15.000 $K_h$=0.1, $H$=20, $B$=5, $I$=16498, $\bar{a}=\frac{H}{2}\alpha$, $=10\alpha$ to EQ (5) gives

$$13.33Peh-5Pev-493=63082\alpha$$

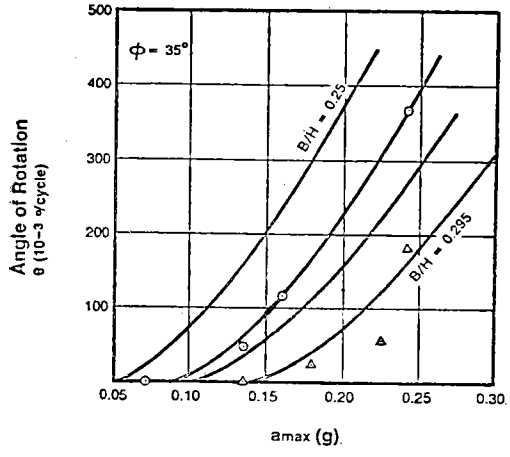


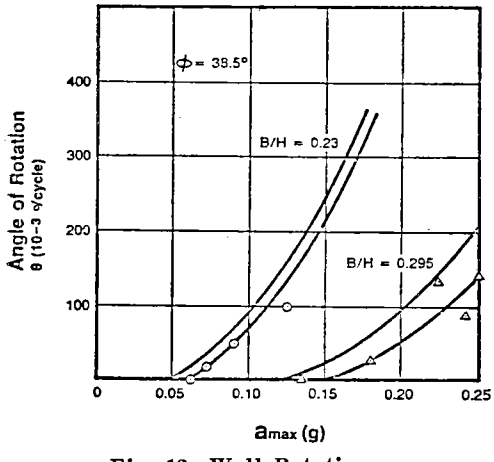


**Fig. 12. Wall Rotation**

$P_{EH}=1/2\,\gamma H^2$ Kae cos $\delta - P_{ah}=1608$

$P_{EV}=P_{EH}\tan\delta=693$

$\alpha=0.277\text{rad/sec}^2=15.87°/\text{sec}^2$

$\theta=t^2=15.87(14/160)^2=0.122°/\text{cycle}$

$\sum\theta=10\times0.122=1.22$ degree

Displacement $=H\sin\theta=20\times12\sin 1.22°$

$=5.1$ inch

It must be recalled that many simplications and assumptions are made in the analysis. The most important ones are the location of the dynamic increment acting at a point one third of the wall height from the top, the center of rotation, and the replacement of the sinusoidal acceleration by step pulses. There were some practical problems as well. It was difficult to apply the desired level of acceleration instantaneously in the tests. There were some time lags and slightly unstable accelerations before the desired levels of acceleration were achieved. At higher levels of acceleration the problem could be serious because the model walls could have moved significantly in those periods of time. The accelerograms generated did not come out perfectly as a sinusoidal function. They were slightly distorted. Walls moved rapidly under higher acceleration causing difficulty in obtaining accurate data. The test container was not sufficiently large enough to eliminate the boundary effect. Undoubtedly many of these factors can be solved and the results improved in the future.

## 6. Summary and Conclusion

A small scale model experiment and an analytical method to evaluate the permanent retaining wall rotation have been presented in this paper. Although the two do not match exactly, the general trends do agree. It is found that there are yield accelerations for rotation just as there are yield acceleration for wall sliding. Walls will not rotate unless the ground accelerations exceed the yield accelerations which become larger for higher factors of safety. The magnitude of rotational angle is found to increase rapidly with the applied ground acceleration, smaller wall base and lower angle of friction. The magnitudes of the rotation of walls may be estimated by the equation of motion. However it tends to overrestimate according to the experimental data. The displacement of the top of the walls can then be estimated. This rotational movement may cause severe displacement at the top of the walls.

## Appendix I.-References

1. Goodman, R.E. and Seed, H.B., "Earthquake Induced Displacement in Sand Embankments," Jour. Soil Mech. and Found. Engrg. Div. ASCE, Vol.92, No. SM 2, March, 1966.

2. Lee, K. L. and Singh, A., "Report of the Direct Shear Cmparative Study," Univ. of Calif, L. A. Nov. 1968.
3. Matsuo, H. and Ohara, S., "Lateral Earth Pressures and Stability of Quay Walls during Earthquakes," Proc. Second World Conference on Earthquake Engineering, Tokyo, Vol. 1, p. 165, 1960.
4. Mononobe, N., "Earthquake Proof Construction of Masonary Dams," Proc. World Engineering Congress Tokyo, Vol. 9, p.275, 1929.
5. Mononobe, N. and Matsuo, H., "On Determination of Earth Pressure during Earthquake," Proc. World Engineering Congress, Tokyo, 1929.
6. Murphy, V., "The Effect of Ground Characteristics on the Aseismic Design of Structures," Second World Conf. on Earthquake Engrg. Tokyo, 1960, pp. 231-247.
7. Nazarian, H.N., and Hadjian, A.H., "Earthquake-Induced Lateral Soil Pressures on Structures," J. Geotech. Engrg. Div. ASCE, Vol. 105, No. GT9, Sept. 1979.
8. Newmark, N.M. "Effects of Earthquakes on Dams and Embankments," Geotechnique, London, Vol. 15, No. 2, 1965, pp. 139-160.
9. Okabe, S., "General Theory of Earth Pressure, "J. Japanese Soc. of Civil Engineers, Vol. 12, No. 1, 1926.
10. Prakash, S. "Soil Dynamics," McGraw-Hill, 1981 pp. 128-170.
11. Rea, D. and Wolfe, W.E., "Earthquake-Induced Permanent Displacement in Model Reinforced Earth Walls," Seventh World Conf. on Earthquake Engrg. Istanbul, Turkey, Sept., 1980.
12. Richards, R.Jr. and Elms, D.G., "Seismic Behavior of Gravity Retaining Walls", J. Geotech. Engrg. Div. ASCE, Vol. 105, No. GT4, April, 1979.
13. Seed, H.B., and Whitman, R.V., "Design of Earth Retaining Structures for Dynamic Loads," Lateral Stresses in the Ground and Design of Earth Retaining Structures, ASCE, 1970, pp. 103-147.
14. Sim, L.C. and Berrill, J.B., "Shaking Table Tests on a Model Retaining Wall," Bull. of the New Zealand Nat. Soc. for Earthquake Engrg. Vol. 12, No. 3, June 1979.

## Appendix Ⅱ.-Notation

The following symbols are used in this paper:

$\bar{a}$ = linear acceleration of the wall
$B$ = base width of walls
$g$ = acceleration of gravity
$H$ = wall height
$I$ = moment of the inertia of walls
$i$ = backfill slope
$K_{AE}$ = dynamic active earth pressure coefficient
$K_h$ = Horizontal acceleration coefficient
$K_r$ = yield acceleration for rotation
$K_s$ = yield acceleration for sliding
$K_v$ = vertical acceleration coefficient
$P_{AE}$ = dynamic active force
$P_a$ = static active force
$P_E$ = dynamic increment of active force
$W$ = wall weight
$\bar{x}$ = horizontal distance from the center of the wall to the toe
$x_1$ = Horizontal distance from the static active force resultant to the toe
$x_2$ = horizontal distance from the dynamic active force resultant to the toe
$\bar{y}$ = vertical distance from the center of the wall to the toe
$\alpha$ = angular acceleration of walls
$\beta$ = slope of the wall to the vertical
$\gamma$ = unit weight of soils
$\delta$ = friction angle between base and soil = $\frac{2}{3}\phi$
$\phi$ = soil friction angle